

Geophysical Research Letters®

RESEARCH LETTER

10.1029/2023GL103055

Key Points:

- We report an undisturbed 6,100-m continuous heat-flow profile from the scientific drilling project SK-2e
- The heat-flow profile recorded a 2 K rise of ground surface temperature in the last five centuries and a 10 K rise since the Last Glacial Maximum
- A basin-scale comparison reveals localized heat-flow anomalies induced by advective heat in deep and confined high-permeability aquifers

Supporting Information:

Supporting Information may be found in the online version of this article.

Correspondence to:

Y. Tian,
tianyuntao@mail.sysu.edu.cn

Citation:

Jiang, G., Tian, Y., Lv, Q., Sandiford, M., Shi, Y., Zou, C., et al. (2023). Ground surface temperature history since the Last Glacial Maximum in Northeast Asia: Reconstructions from the borehole geotherms of the International Continental Scientific Drilling Program. *Geophysical Research Letters*, 50, e2023GL103055. <https://doi.org/10.1029/2023GL103055>

Received 30 JAN 2023

Accepted 10 APR 2023

Ground Surface Temperature History Since the Last Glacial Maximum in Northeast Asia: Reconstructions From the Borehole Geotherms of the International Continental Scientific Drilling Program

Guangzheng Jiang^{1,2} , Yuntao Tian^{3,4} , Qingtian Lv⁵ , Mike Sandiford⁶, Yizuo Shi⁷, Changchun Zou⁸ , Feng Ma⁹, Chenglong Deng¹⁰ , Lijuan He¹⁰, and Shengbiao Hu¹⁰

¹State Key Laboratory of Oil and Gas Reservoir Geology and Exploitation, Chengdu University of Technology, Chengdu, China, ²College of Energy, Chengdu University of Technology, Chengdu, China, ³Guangdong Provincial Key Laboratory of Geodynamics and Geohazards, School of Earth Sciences and Engineering, Sun Yat-sen University, Zhuhai, China, ⁴Southern Marine Science and Engineering Guangdong Laboratory (Zhuhai), Zhuhai, China, ⁵China Deep Exploration Center, China Geological Survey & Chinese Academy of Geological Sciences, Beijing, China, ⁶School of Earth Sciences, University of Melbourne, Parkville, VIC, Australia, ⁷PetroChina Research Institute of Petroleum Exploration & Development, Beijing, China, ⁸China University of Geosciences, Beijing, China, ⁹Institute of Hydrogeology and Environmental Geology, Chinese Academy of Geological Science, Shijiazhuang, China, ¹⁰State Key Laboratory of Lithospheric Evolution, Institute of Geology and Geophysics, Chinese Academy of Sciences, Beijing, China

Abstract Past ground surface temperature (GST), one of the important aspects of paleoclimate reconstructions, can be inverted from borehole temperature measurements. Here, we report continuous 6,100-m temperature logs in the International Continental Scientific Drilling Program SK-2e. We inverted the past GST changes from upper borehole temperature logging (<600 m). Below this depth, localized fluid flow masks the paleoclimate record. Inversions yield an approximately 2 K GST rise since 0.1–0.6 Kyr BP and an approximately 10 K rise since 20 Kyr BP. Assuming a ±5 K influence from the deep groundwater flow, the inverted temperature rise has varied between 8 and 12 K since 20 Kyr BP, which is consistent with previous reports since the Last Glacial Maximum. Our results emphasize the potential of borehole heat-flow profiles as a record of climate changes and the importance of climate correction for heat-flow determinations.

Plain Language Summary Temperatures within the shallow boreholes are perturbed by changes in ground surface temperature (GST) in response to paleoclimate variations and anthropogenic land use. The GST varies at different time scales, and these variations penetrate different depths underground. Thus, the borehole temperatures can be used for reconstructing the history of ground surface temperatures. Based on borehole geotherms of the International Continental Scientific Drilling Program in Northeast Asia, the past GST changes since the Last Glacial Maximum were inverted. The results show a ~2 K surface temperature rise during 0.1–0.6 Kyr BP and a ~10 K rise since 20 Kyr BP, which is consistent with previous independent estimates.

1. Introduction

The Earth's temperature field is one of the controlling factors of petrophysical properties, such as seismic velocity and rheological strength. Borehole geothermal measurements open a window into the thermal regime of deep Earth, allowing extrapolations to heat flow and geotherms, with the combination of thermal conductivity and heat production measurements (Furlong & Chapman, 2013). Furthermore, the temperatures within the shallow boreholes are often perturbed by groundwater movement (Guillou-Frottier et al., 2013; Jessop, 1993) and changes in ground surface temperature (GST) induced by paleoclimate variations and anthropogenic land use (Gosnold et al., 2011; Majorowicz et al., 2012). Paleoclimatic signatures could perturb equilibrium heat flow densities to more than 2 km (Beltrami et al., 2014). Therefore, detailed borehole geothermal studies have the potential to provide unique constraints on both deep-earth thermal processes and GST changes.

Available global heat-flow and paleoclimate studies primarily rely on shallow (<1,000 m) boreholes (Cuesta-Valero et al., 2021; Davies, 2013; Huang et al., 2000). Long-term climate changes cause significant perturbations in the measured heat flow, leading to deviations in the global heat-flow data set. Climatic perturbations, which are considered noise to determine the heat flow, can be used for GST reconstruction (Cermak and Bodri, 2011).

© 2023 The Authors.

This is an open access article under the terms of the Creative Commons Attribution-NonCommercial License, which permits use, distribution and reproduction in any medium, provided the original work is properly cited and is not used for commercial purposes.

The theories and technologies for reconstructing the paleoclimate based on borehole temperature have been developed (Cuesta-Valero et al., 2021; Davies, 2013; Huang et al., 2000). However, GST reconstructions using this method remain limited. Only dozens of the global data set, including 70,000 borehole temperature logs, have been successfully utilized. One of the primary reasons is that the borehole temperature is inevitably influenced in part by groundwater activities (Jiang et al., 2016; Mottaghy et al., 2005). Additionally, vertical distributions of heat production are often estimated by empirical correlations between heat production and the rock type, with limited constraints from measurements. Superdeep continental scientific drilling boreholes are excellent opportunities to constrain the lithospheric thermal structure and to explicitly establish the relationship between heat-production variation and depth.

The SK-2e borehole is the current deepest scientific drilling project in Northeast Asia, with a depth of 7,018 m, from which continuous 4,134 m cores have been recovered. The SK-2e is located in the Songliao Basin, Northeast China, approximately 1,200 km west of the Pacific subduction zone (Figure 1a). This superdeep scientific drilling provides unique geothermal information on the inner Earth's temperature, heat flow, and thermal structure. Moreover, it is also valuable in reconstructing past GST changes in Northeast Asia. This paper reports the 6,400-m continuous temperature logging, thermal conductivity, heat production, and vertical heat-flow profile from SK-2e. We also interpret the heat-flow variations in terms of the GST history and groundwater movement.

2. Study Site

The Songliao Basin, where the SK-2e borehole was targeted, formed on the pre-Triassic basement and experienced three filling stages of the syn-rift (150–105 Ma), post-rift (105–79.1 Ma) and structural inversion (79.1–64 Ma), with sedimentary thickness up to 6 km (Wang et al., 2013, 2016). The basin includes five subunits, including Western Slope, Central Depression (where SK-2e is located), Northern Plunge, Southeastern Uplift, and Southwestern Uplift (Figure 1b).

The previous heat flow data show that the basin is characterized by high heat flow, with a mean of $70.9 \pm 14.4 \text{ mW m}^{-2}$ (Shi et al., 2018; Wu & Xie, 1985). The estimated vertical heat-flow profiles exhibit a gradually increasing trend from 0 to approximately 1,000 m and positive anomalies from 1,000 to 2,000 m. A purely conductive heat flow cannot explain the observed anomalous heat-flow trends. Besides, as shown in Figure 1c, the anomalies coincide distinctly with the high-porosity/permeability hydrocarbon reservoirs between the lower K₂n to the upper K₂q (Wang et al., 2013), suggesting that they stem from advective heat transport associated with fluid migration. Significant vertical components or horizontal fluid movements in the inclined layer could exist in these high-porosity/permeability zones. Horizontal flow in deep confined aquifers is likely to be eastward in the Songliao Basin as the elevation of the western margin is approximately 900–1,200 m higher than the eastern, leading to correspondingly higher hydraulic heads (Zhu, 2011). Furthermore, previously published data indicate an increasing trend of heat flow from west to east, with values increasing from 44.4 to 95.0 mW m⁻² (Wu & Xie, 1985). This trend further supports a regional aquifer signal consisting of eastward-directed flow. The westerly boreholes (e.g., S2 and K2) exhibit the lowest heat-flow values, while higher heat-flow values are observed in boreholes G507, TS1, Z12, and X4 located in the central basin, where the aquifers extend to deeper levels. The fact that the heat flow anomalies have a wide depth range and continuous variation suggests that they are stable and long-lasting over periods of at least ten thousand years. Although the contribution of the advective heat transport within aquifers is not yet quantitatively resolved, this finding suggests supports the feasibility of GST reconstruction from a borehole with a local thermal anomaly. Finally, marking the start of the post-rift thermal subsidence phase of the Songliao Basin, K₂q and the upper strata are unaffected by syn-depositional faulting (Wang et al., 2013), mitigating against the influence of vertical fluid migration (Figure 1c). Thus, SK-2e is of great significance in reconstructing the GST and confirming basin-scale fluid migration.

3. Data Collection and Observations

3.1. Temperature Logging

The temperature logging of the SK-2e borehole was conducted on 25 March 2016, and 7 August 2019. During the second set of measurements, the temperature sensor reached only 6,130 m due to mud obstacles in the lowest section of the borehole. Borehole temperature logging was performed using a PPS71 geothermal memory tool, equipped with a platinum resistance temperature sensor (maximum temperature: 350°C) and a 10,000-m-long cable. The system allows temperature recordings with a 0.01 K sensitivity, a 0.2 K accuracy, and less than 2 s

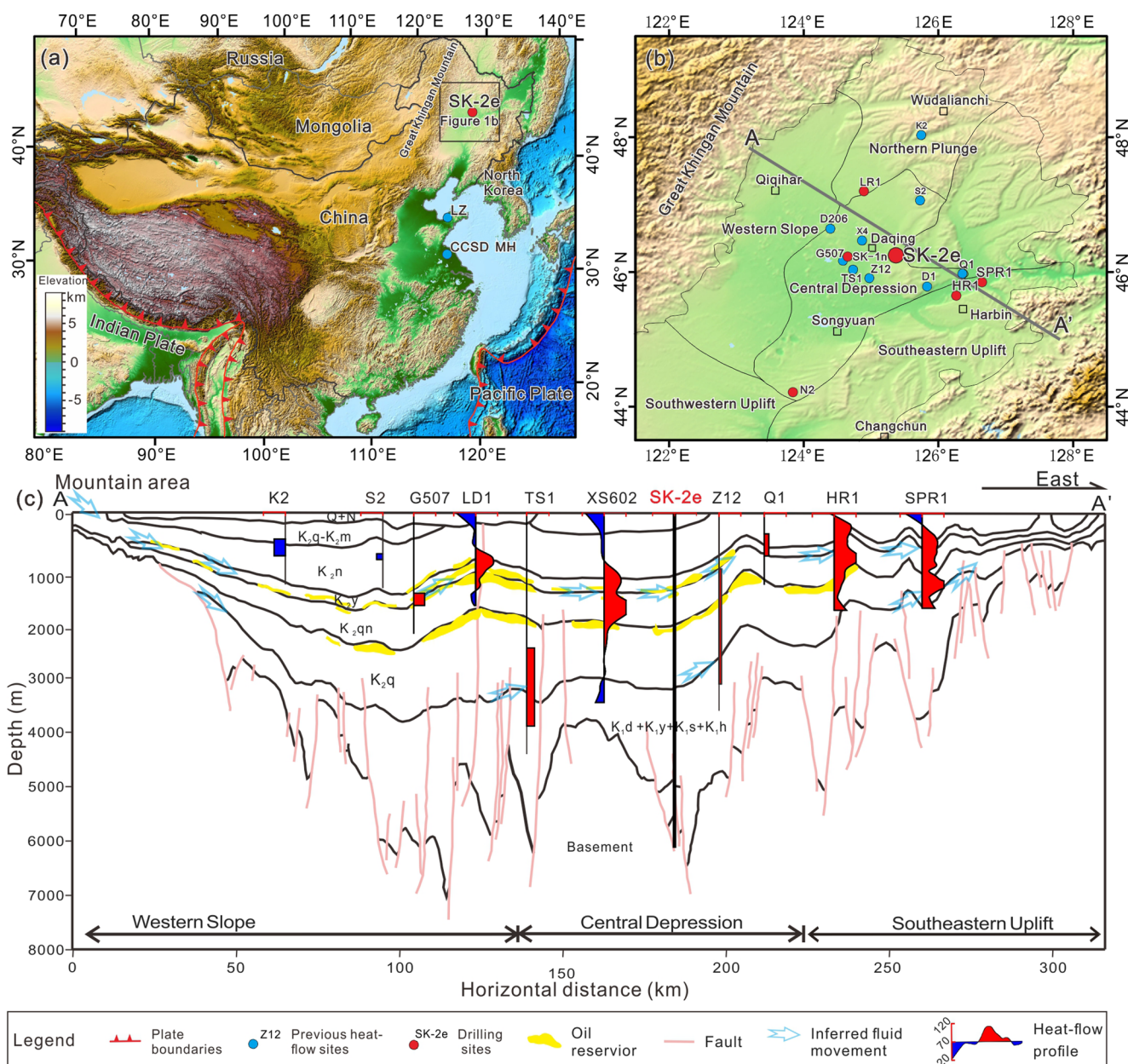


Figure 1. (a) Tectonic setting and topography surrounding SK-2e. (b) Subunits of the Songliao Basin, location of SK-2e, and previous heat-flow measurements (Wu & Xie, 1985). SK-1n and N2 are complementary core samples. The CCSD-MH (Chinese Continental Scientific Drilling Main Hole) and LZ show the location of the previous continuous heat-flow profile penetrating the crystalline basement. (c) Stratigraphic cross-section of AA', interpreted with borehole-constrained seismic data (modified from Wang et al. (2013)), and simplified vertical heat-flow profile along the cross-section. Heat flows that are higher and lower than the background value of 70 mW m^{-2} are filled in red and blue, respectively. Formation symbols: K₁h = Huoshiling, K₁s = Shahezi, K₁y = Yingcheng, K₁d = Denglouku, K₁q = Quantou, K₁qn = Qingshankou, K₂y = Yaojia, K₂n = Nenjiang, K₂s = Sifangtai, K₂m = Mingshui, and Q = Quaternary (Deng et al., 2013).

response time. The recording time interval was 0.5 s, and a downward logging speed of 6 m/min was adopted to ensure sufficient time for the sensor to record the temperature without delay.

The first temperature log was recorded 35 days after drilling to a depth of approximately 4,200 m, and the second log was recorded 507 days after drilling had finished, at a depth of 7,018 m. The repeated loggings indicate a distinct thermal recovery process, with the recovered temperatures of the two logs crossing at approximately 1,400 m. The second temperature log records an average temperature gradient of 36.0 mK m^{-1} compared with 31.1 mK m^{-1} in the first log. To assess the temperature recovery, we compare the measured temperatures with the values collected from drill stem tests (DSTs), which are widely used in the oil industry to estimate equilibrium

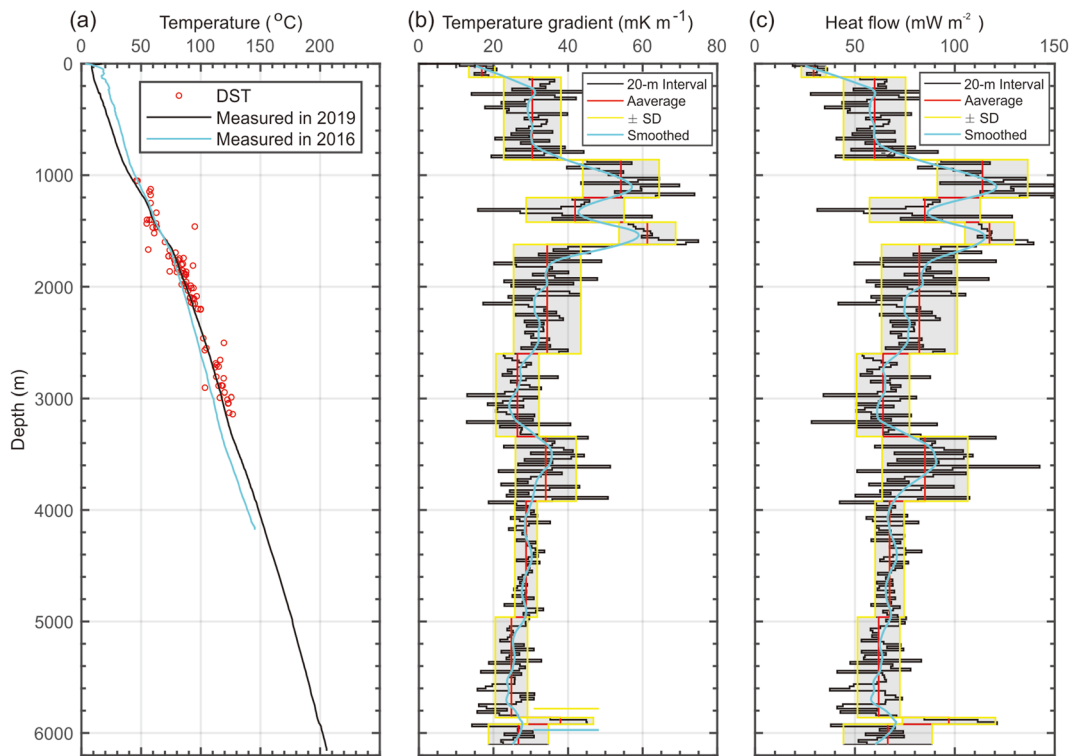


Figure 2. (a) Temperature log at 35 days after drilling that stopped halfway in 2016 and 507 days after drilling that finished in 2019. (b) Temperature gradient at 20-m intervals. (c) Heat flow vertical variations. The red stepped line is the arithmetic mean of the temperature gradient/heat flow data of each segment. The shaded area is the ± 1 standard deviation (SD). The cyan line is the linear least squares smoothed temperature gradient and heat flow in the 100-m interval.

temperatures. We note that the second temperature log is generally consistent with the DST temperature estimates (see Figure 2a), giving confidence that it approximates the steady-state temperature profile.

The second log shows the temperature abruptly decreases from 17.2 to 8°C in the uppermost 13.6 m, which is consistent with seasonal and annual temperature GST variabilities expected for mid-late summer logging. At depths greater than 20 m, the temperature continuously increases to 205°C at 6,130 m. The 20-m interval-averaged temperature gradient varies between 10.9 and 74.4 mK m⁻¹ with distinct peaks at depths of approximately 1,200 and 1,600 m. In the shallowest 1,000 m, the gradient increases with depth, most prominently in the first 120 m and between 860 and 1,000 m. Near the surface (20–120 m), the temperature gradient is as low as 16.7 ± 3.5 mK m⁻¹. Between 120 and 860 m, it averages 30.4 ± 7.7 mK m⁻¹. Four apparent positive temperature gradient anomalies can be distinguished in Figure 2b.

3.2. Thermal Conductivity and Heat Flow

Thermal conductivity measurements were performed on samples collected from the SK-2e ($n = 404$) and adjacent boreholes SK-1n ($n = 148$) and N2 ($n = 11$). Because cores were not recovered during drilling for the upper section (less than 2,800 m) of the SK-2e borehole, samples from the adjacent borehole SK-1n (~60 km west of SK-2e and 0–2,000 m continuous cores) and N2 (~150 km southwest of SK-2e) were collected to complement the data set. The thermal conductivity was measured by a high-precision non-contact optical scanning technology (Popov et al., 1999). Measurements were performed on dry cores along a scanning line on a diametral plane at ambient temperature. The measured values were corrected to the in situ conditions through water-saturated (porosity) (Beardmore et al., 2001) and temperature corrections (Sekiguchi, 1984). The porosity was obtained from the neutron log (Chen, 2018; Zou et al., 2018). A pressure correction was neglected because the maximum thermal conductivity increase remains within 1.3%, according to Kappelmeyer and Haenel (1974).

Below 2,800 m, the in-situ thermal conductivity is adopted. Above 2,800 m, the thermal conductivity is referred to as the average value of the SK-1n and N2 for the corresponding formations (i.e., K_2q to Q , as illustrated by the applicable Creative Commons License

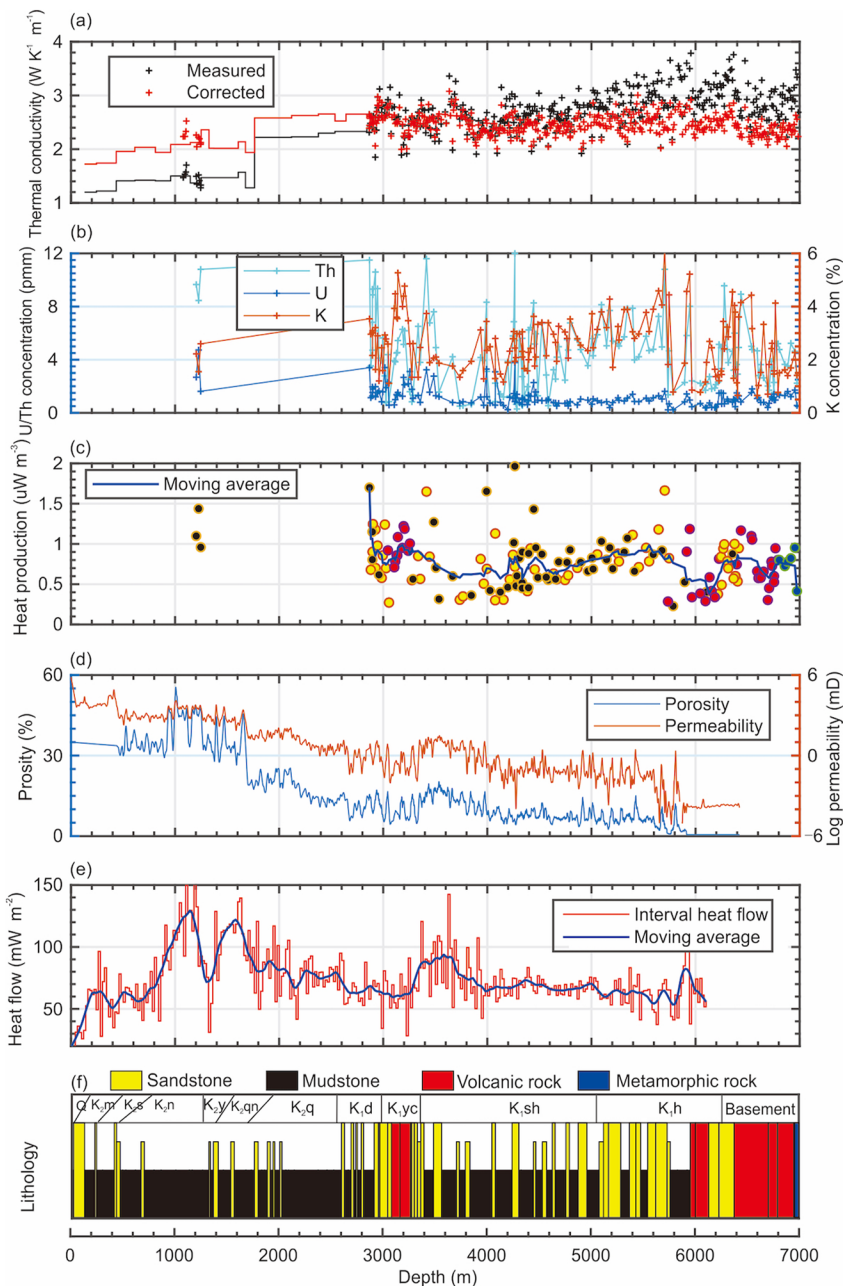


Figure 3. (a) Thermal conductivity, (b) U-Th-K concentration, (c) heat production, (d) porosity and permeability, (e) heat flow, and (f) stratigraphic column of SK-2e. The different colored spots in (c) present the rock types as in (f).

stepped lines in Figure 3a). The measured thermal conductivity values range from 2.24 to 3.56 W m⁻¹ K⁻¹ and exhibit a slightly increasing trend with the depth (Figure 3a). Water-saturated correction of thermal conductivity is essential for the samples from the shallow high-porosity stratum, with a maximum correction as high as 40%. The porosity decreases to ~2% at the bottom of the hole, where the water-saturated effect decreases to less than 1%. The maximum temperature correction of thermal conductivity is about -18% at the maximum measured depth of 6,100 m (205°C). The measured and fully corrected profiles are shown in Figure 3a. The fully corrected thermal conductivity tends to increase with depth in the interval of 0–2,000 m and stabilizes thereafter due to the combined effects of declining porosity and increasing temperature.

The heat flow was calculated as the product of the least squares smoothed temperature gradient and the thermal conductivity, derived at approximately 20-m depth intervals, as shown in Figures 2c and 3e. The vertical heat-flow

values range from 18 to 170 mW m⁻², with moving average estimates mostly in the range of 50–80 mW m⁻². An increasing trend is observed in the shallower section of the borehole, and a gradually decreasing trend occurs in the deeper section. The heat flow increases from approximately 28–32 mW m⁻² in the uppermost 120 m to 45–60 mW m⁻² in the 120–860 m interval and then rises to 110–120 mW m⁻² from 860 to 1,600 m. Below this depth interval, the heat flow gradually decreases to 65 mW m⁻² at a depth of ~3,340 m. The depth interval of 3,340–3,920 m reveals an apparent anomaly with a magnitude of 86 mW m⁻². Below 4,000 m, the heat flow exhibits more minor fluctuations and relatively constant heat flow, with an average of 66 mW m⁻².

3.3. Heat Production

The heat-production value is calculated through the empirical equation (Birch, 1954):

$$A = 10^{-5} \rho(9.52C_U + 2.56C_{Th} + 3.48C_K) \quad (1)$$

where A is the heat production in $\mu\text{W m}^{-3}$; ρ is the density in kg m^{-3} ; C_U and C_{Th} are the U and Th concentrations, respectively, in ppm, and C_K is the K content as a percentage. The uranium and thorium concentrations were acquired through inductively coupled plasma mass spectrometry, and the potassium concentration was determined by X-ray fluorescence spectroscopy. The density was obtained from the neutron log (Chen, 2018; Zou et al., 2018). The U, Th, and K concentrations in 158 core samples were measured from 2,800 m to the bottom at depth intervals of 20–50 m.

The vertical variations in the U, Th, and K concentrations and heat production with depth are shown in Figures 3b and 3c. Overall, the samples show relatively low U, Th, and K concentrations, with a high Th/U ratio, with a mean of 4.3 ± 2.8 , which is much greater than the global mean of 2.5. The heat production values estimated from the U, Th, and K concentrations are also low (sandstones: $0.75 \pm 0.31 \mu\text{W m}^{-3}$; mudstones: $0.81 \pm 0.36 \mu\text{W m}^{-3}$; volcanic rocks: $0.75 \pm 0.29 \mu\text{W m}^{-3}$; and metamorphic rocks: $0.76 \pm 0.18 \mu\text{W m}^{-3}$). No distinct differences in the concentrations of the radiogenic elements, heat production, or Th/U ratio are observed among rock types (Figure 3c). The integrated heat production contribution in the upper 6,000-m sedimentary cover is equivalent to ~5 mW m⁻² in heat-flow terms. The characteristic heat-flow value of 66 mW m⁻² obtained in the deepest borehole section yields an equilibrium surface heat value of 71 mW m⁻² after the heat production contribution is taken into account.

4. GST Inversion Method and Input Data

Given the similar lithology and rock properties throughout the SK-2e borehole (Figures 3d and 3f), the lower heat flow (28–60 mW m⁻²) in the upper 860 m than the deeper sections (Figures 2c and 3e) probably implies a significant perturbation from equilibrium, likely due to GST changes, which are explored in the section below.

4.1. Methodology

The forward model of borehole climate reconstruction is based on pure conductive heat transfer in a homogeneous semi-infinite half-space porous medium. We use finite difference techniques to solve the 1-D time-dependent heat conduction Equation 2, with the up ($z = z_0$) temperature boundary (T_{GS}) and bottom ($z = z_{max}$) constant heat flow boundary conditions set as Equations 3 and 4, respectively.

$$(\rho c)_e \frac{\partial T}{\partial t} + \frac{\partial}{\partial z} \left(\lambda_e \frac{\partial T}{\partial z} \right) - A = 0 \quad (2)$$

$$T(z_0, t) = T_{GS}(t) \quad (3)$$

$$\frac{\partial T}{\partial z}(z_{max}) = \frac{q_b}{\lambda_e} \quad (4)$$

where the index e marks effective properties that describe the rock–fluid two-phase system as given by $(\rho c)_e = \varphi \rho_w c_w + (1 - \varphi) \rho_m c_m$, where the index of w and m represent water and matrix, and φ represents porosity. q_b is the assumed basal heat flow at z_{max} .

To obtain a quantitative and stable GST history path, we performed a 1-D Tikhonov deterministic method inversion and a Bayesian stochastic approach with a Metropolis-Hastings Markov Chain Monte Carlo (MCMC)

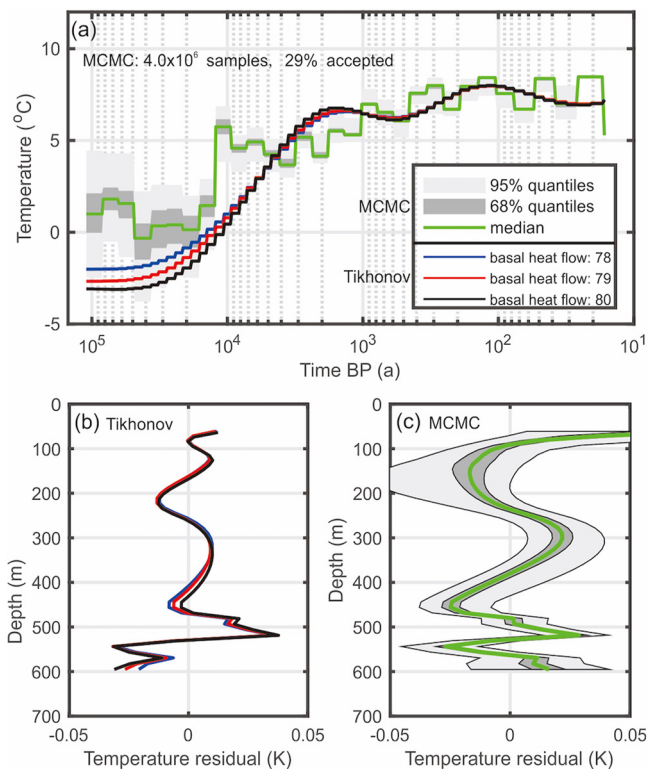


Figure 4. Tikhonov inversions and Markov Chain Monte Carlo (MCMC) inversions of the SK-2e geothermal data in 60–600 m intervals. (a) Estimated ground surface temperature history using the Tikhonov and MCMC inversion methods. (b, c) Temperature residuals of Tikhonov and MCMC inversions.

tion results in several abrupt and possibly excessive temperature changes of magnitude ~ 5 K on centennial to millennial time scales at approximately 4–30 Kyr BP. The Tikhonov inversion aims to derive one “optimum” model, which may produce many equivalent models (Mottaghy et al., 2013; Rath & Mottaghy, 2007), whereas MCMC methods yield a joint posterior distribution of the parameters. Considering GST history inversions highlight only the low-frequency variability (Pollack et al., 2006), the smooth Tikhonov inversions can reflect the past GST variations, probably better than the variable MCMC results. Unless specified, the reconstructed GST in the following sections refers to Tikhonov inversions.

The GST reconstructions for the period from 0.1 to 30 Kyr BP are consistent with previous studies. The use of temperature intervals at depths greater than 60 m means that our inversions are not sensitized to GST changes over the last century. We note that the Tikhonov inversions are consistent with the last five-century cumulative GST change of +2 K (Figure 4a), which is consistent with the value in southeastern Australia (Beardsmore et al., 2017) and slightly larger than the average of 1.1 K in the Northern Hemisphere (Huang et al., 2000). The results also exhibit a 10 K GST rise from the minimum temperature during the Last Glacial Maximum, which is consistent with the scientific drilling in Olkiluoto (Kukkonen et al., 2011), but lower than those determined in northern Poland (~ 13 K) (Majorowicz & Safanda, 2008) and northwestern Russia (12–13 K) (Demezhko & Shchapov, 2001).

The fact that the inversions diverge for periods greater than 30 Kyr BP means that our confidence in the GST histories before the Last Glacial Maximum is low. This may in part reflect the impact of thermal effects of transient fluid migration in the deeper part of the section modeled in GST inversions. Furthermore, because the top 40 m of the temperature log is likely impacted by groundwater flow and seasonal temperature variations, these suggest the decreased temperature in the last tens of years in both inversions is not considered reflective of climate change.

algorithm (code from https://github.com/volkerrath/BTL_2019) (Rath & Mottaghy, 2007; Rath et al., 2012). The Tikhonov method estimated the GST history by a regularized least-squares procedure, with the generalized cross-validation method’s optimum regularization parameter. The MCMC inversion used the delayed rejection adaptive Monte Carlo (DRAM) algorithm (Haario et al., 2006).

4.2. Input Parameters

The input parameters for the model include the temperature log, thermal conductivity, density, porosity, heat production (presented above), and matrix heat capacity (Zhu, 2011), along with the current annual mean surface temperature of 8°C. Forward models were run for a 6,000-m profile to avoid potential boundary effects, whereas inverse models were run for the 60–600 m interval, where an abnormally low heat flow implies a GST perturbation (as discussed above). Models were run using a basal heat flow of 78–80 mW m⁻², similar to the average of observations at depths of 600–1,200 m, which is below the interval used for GST reconstruction.

5. Results and Discussions

5.1. Inversed GST History

The Tikhonov method suggests a continuous and smoothed GST increase since 40–30 Kyr BP (Figure 4a). The MCMC inversion shows similar GST histories between 30 and 0.1 Kyr BP, based on 4.0×10^6 samples, of which 29% were accepted. At earlier times, the modeling results of the two methods are different. The inverted vertical temperature profile fits well with the observed values, with temperature residuals smaller than 0.05 K (Figures 4b and 4c).

GST histories estimated using both methods show overall warming of approximately 10 K from approximately 20 Kyr. We note the MCMC inversion

5.2. Uncertainties From Local Heat Convection

The inversions discussed above show that even in the presence of localized basin-scale fluid movements, the borehole temperature can still record the past GST signals. The new thermal equilibrium was reached after the stable and long-lasting fluid migrations. The heat effect of fluid migration is equivalent to the lower boundary of variable heat flow. Furthermore, most climate reconstruction boreholes are only a few hundred meters deep (Beltrami et al., 2006), despite the recorded temperature period revealing little hydrologic activity, and the deeper interval is uncertain. Local fluid activity may exist in most circumstances. The local fluid convection beneath the recorded maximum depth (particularly far from the borehole bottom) would not erase the GST history signals, as shown by the consistency among the GST reconstructions (Beltrami et al., 2017; Erkan et al., 2019; Vogt et al., 2014). To further validate the above discussion, parameter numerical simulation experiments were conducted. The thermal effect of fluid activity was equivalent to a sharp increase in temperature at the corresponding depth, forming a temperature field, which was then used as input for inversion. The results showed that assuming a ± 5 K groundwater temperature change at depths below 1 km, the inverted temperature rise varies between 8 and 12 K since 20 Kyr BP. This result remains consistent with this and previous studies (see Supporting Information S1 for details). Although utilizing thermo-hydro modeling would be helpful in testing and removing the effects of fluid convection (Vogt et al., 2014), it requires far more computational resources and involves more uncertainties in additional hydraulic parameters for modeling the fluid flow.

5.3. Affecting Heat Flow Estimate

The aforementioned result also serves as a reminder for utilizing caution when determining heat-flow data from shallow boreholes. The borehole depths should be taken into account when analyzing the heat-flow distribution, particularly for sedimentary basins. For instance, advective fluid flow and paleoclimate mask the deep heat-flow signal, as shown by the increasing trend of heat flow from the western to central areas of the Songliao Basin (Figure 1c). In this regard, the SK-2e shows the importance of superdeep boreholes in establishing criteria for discerning the relative contributions of these different factors to the observed temperature gradients and heat flow. A detailed analysis of the vertical variation in the heat flow has implications for obtaining high-quality heat-flow data to remove the effect of lateral convective heat and GST changes. The newly determined heat flow is consistent with the values determined from other deep boreholes penetrating the crystalline basement in eastern China (Figure 1a), including CCSD-MH, ($\sim 66 \text{ mW m}^{-2}$ at 4,600 m) (He et al., 2009), and borehole LZ ($\sim 69 \text{ mW m}^{-2}$ at $\sim 3,500$ m) (Jiang et al., 2016). The consistency among the three heat-flow values implies that heat flow in eastern China is quite typical for a continental interior.

6. Conclusions

The equilibrium temperature log and thermal conductivity data yield a 6,100-m vertical heat-flow profile in SK-2e. The lower section of the profile exhibits a representative background heat-flow value of 66 mW m^{-2} from 4,000 to 6,000 m, corresponding to a surface value of 71 mW m^{-2} when the $\sim 5 \text{ mW m}^{-2}$ heat-production contribution in the upper layers is factored in. The heat-flow profile in the uppermost 600 m mostly recorded a 2 K rise of GST in the last five centuries (0.1–0.6 Kyr BP) and a 10 K rise of GST since the Last Glacial Maximum (~ 30 –20 Kyr BP). These results also suggest that the paleoclimate effects have reduced the apparent heat-flow data measured in the uppermost 1 km by as much as 10–20 mW m^{-2} . Significant localized positive heat-flow anomalies within the deeper segments agree well with the identified high-porosity/permeability zones. A comparison of the surrounding vertical heat-flow profiles indicates that the heat-flow anomalies are regionally distributed in the Songliao Basin and can be attributed to differences in the advective heat transport. Our study not only emphasizes the importance of high-quality geothermal temperature logging data in reconstructing past climates but also reveals their potential for climate correction for heat-flow determinations.

Data Availability Statement

All the observation data are provided in Data Sets S1–S9 and are available on FigShare (<https://doi.org/10.6084/m9.figshare.22273054.v4>).

Acknowledgments

This research is supported by the National Natural Science Foundation of China (No: 42004076, 42130809, 41888101, and 42074096) and Southern Marine Science and Engineering Guangdong Laboratory (Zhuhai) (No: SML2021SP315). We thank Professor Chengshan Wang for his help during the temperature logging. Constructive reviews from Dr. Volker Rath and an anonymous reviewer, and handling editor Dr. Harihar Rajaram clarified many points in this manuscript.

References

- Beardsmore, G., Sandiford, M., Gordon, K., Mclean, M., & McLaren, S. (2017). Heat flow and inferred ground surface temperature history at Tynong North, southeastern Australia. *Australian Journal of Earth Sciences*, 64(6), 1–15. <https://doi.org/10.1080/08120099.2017.1362663>
- Beardsmore, G. R., Cull, J. P., & Cull, J. P. (2001). *Crustal heat flow: A guide to measurement and modelling* (pp. 132–133). Cambridge University Press.
- Beltrami, H., Gonzalez-Rouco, J. F., & Stevens, M. B. (2006). Subsurface temperatures during the last millennium: Model and observation. *Geophysical Research Letters*, 33(9), L09705. <https://doi.org/10.1029/2006gl026050>
- Beltrami, H., Matharao, G. S., Smerdon, J. E., Illanes, L., & Tarasov, L. (2017). Impacts of the Last Glacial Cycle on ground surface temperature reconstructions over the last millennium. *Geophysical Research Letters*, 44(1), 355–364. <https://doi.org/10.1002/2016gl071317>
- Beltrami, H., Matharao, G. S., Tarasov, L., Rath, V., & Smerdon, J. E. (2014). Numerical studies on the impact of the Last Glacial Cycle on recent borehole temperature profiles: Implications for terrestrial energy balance. *Climate of the Past*, 10(5), 1693–1706. <https://doi.org/10.5194/cp-10-1693-2014>
- Birch, F. (1954). Heat from radioactivity. *Nuclear geology*, 8, 148–174.
- Cermak, V., & Bodri, L. (2001). Climate reconstruction from subsurface temperatures demonstrated on example of Cuba. *Physics of the Earth and Planetary Interiors*, 126(3–4), 295–310. [https://doi.org/10.1016/s0031-9201\(01\)00262-x](https://doi.org/10.1016/s0031-9201(01)00262-x)
- Chen, T. (2018). The study of logging response characteristic and mechanism of ultra-deep borehole core based on the Scientific Drilling in Songliao Basin. MA thesis, Jilin University, (in Chinese).
- Cuesta-Valero, F. J., García-García, A., Beltrami, H., González-Rouco, J. F., & García-Bustamante, E. (2021). Long-term global ground heat flux and continental heat storage from geothermal data. *Climate of the Past*, 17(1), 451–468. <https://doi.org/10.5194/cp-17-451-2021>
- Davies, J. H. (2013). Global map of solid Earth surface heat flow. *Geochemistry, Geophysics, Geosystems*, 14(10), 4608–4622. <https://doi.org/10.1002/ggge.20271>
- Demezhko, D. Y., & Shchapov, V. A. (2001). 80,000 years ground surface temperature history inferred from the temperature-depth log measured in the superdeep hole SG-4 (the Urals, Russia). *Global and Planetary Change*, 29(3–4), 230. [https://doi.org/10.1016/s0921-8181\(01\)00091-1](https://doi.org/10.1016/s0921-8181(01)00091-1)
- Deng, C. L., He, H. Y., Pan, Y. X., & Zhu, R. X. (2013). Chronology of the terrestrial upper Cretaceous in the Songliao Basin, northeast Asia. *Palaeogeography, Palaeoclimatology, Palaeoecology*, 385, 44–54. <https://doi.org/10.1016/j.palaeo.2012.07.028>
- Erkan, K., Akkoyunlu, B., Inal, M. O., Balkan-Pazvantoglu, E., & Tayanc, M. (2019). Twentieth-century paleoclimatic modeling of borehole temperatures in western and Central Anatolia regions, Turkey. *International Journal of Earth Sciences*, 108(4), 1137–1146. <https://doi.org/10.1007/s00531-019-01698-7>
- Furlong, K. P., & Chapman, D. S. (2013). Heat flow, heat generation, and the thermal state of the lithosphere. *Annual Review of Earth and Planetary Sciences*, 41(1), 385–410. <https://doi.org/10.1146/annurev.earth.031208.100051>
- Gosnold, W., Majorowicz, J., Klenner, R., & Hauck, S. (2011). Implications of post-glacial warming for northern Hemisphere heat flow. *GRC Transactions*, 35, 14–19.
- Guillou-Frottier, L., Carré, C., Bourgine, B., Bouchot, V., & Genter, A. (2013). Structure of hydrothermal convection in the Upper Rhine Graben as inferred from corrected temperature data and basin-scale numerical models. *Journal of Volcanology and Geothermal Research*, 256, 29–49. <https://doi.org/10.1016/j.jvolgeores.2013.02.008>
- Haario, H., Laine, M., Mira, A., & Saksman, E. (2006). DRAM: Efficient adaptive MCMC. *Statistics and Computing*, 16(4), 339–354. <https://doi.org/10.1007/s11222-006-9438-0>
- He, L., Hu, S., Yang, W., & Wang, J. (2009). Radiogenic heat production in the lithosphere of Sulu ultrahigh-pressure metamorphic belt. *Earth and Planetary Science Letters*, 277(3–4), 525–538. <https://doi.org/10.1016/j.epsl.2008.11.022>
- Huang, S., Pollack, H. N., & Shen, P. (2000). Temperature trends over the past five centuries reconstructed from borehole temperatures. *Nature*, 403(6771), 756–758. <https://doi.org/10.1038/35001556>
- Jessop, J. A. M. A. (1993). Relation between basement heat flow and thermal state of the sedimentary succession of the Alberta Plains. *Bulletin of Canadian Petroleum Geology*, 41(3), 358–368.
- Jiang, G., Tang, X., Rao, S., Gao, P., Zhang, L., Zhao, P., & Hu, S. (2016). High-quality heat flow determination from the crystalline basement of the south-east margin of North China Craton. *Journal of Asian Earth Sciences*, 118, 1–10. <https://doi.org/10.1016/j.jseas.2016.01.009>
- Kappelmeyer, O., & Haenel, R. (1974). Geothermics with special reference to application. In *Geoexploration monographs series 4*. Gebrueder Borntraeger.
- Kukkonen, I. T., Rath, V., Kivek S. L., Afanda, J., & Ermak, V. (2011). Geothermal studies of the Outokumpu Deep Drill Hole, Finland: Vertical variation in heat flow and palaeoclimatic implications. *Physics of the Earth and Planetary Interiors*, 188(1–2), 9–25. <https://doi.org/10.1016/j.pepi.2011.06.002>
- Majorowicz, J., Gosnold, W., Gray, A., Safanda, J., Klenner, R., & Unsworth, M. (2012). Implications of post-Glacial warming for northern Alberta heat flow-correcting for the underestimate of the geothermal potential. *GRC Transactions*, 36, 693–698.
- Majorowicz, J., & Safanda, J. (2008). Heat flow variation with depth in Poland: Evidence from equilibrium temperature logs in 2.9-km-deep well Torun-1. *International Journal of Earth Sciences*, 97(2), 307–315. <https://doi.org/10.1007/s00531-007-0210-2>
- Mottaghay, D., Schellschmidt, R., Popov, Y. A., Clauer, C., Kukkonen, I. T., Nover, G., et al. (2005). New heat flow data from the immediate vicinity of the Kola super-deep borehole: Vertical variation in heat flow confirmed and attributed to advection. *Tectonophysics*, 401(1–2), 119–142. <https://doi.org/10.1016/j.tecto.2005.03.005>
- Mottaghay, D., Schwamborn, G., & Rath, V. (2013). Past climate changes and permafrost depth at the Lake El'gygytgyn site: Implications from data and thermal modeling. *Climate of the Past*, 9(1), 119–133. <https://doi.org/10.5194/cp-9-119-2013>
- Pollack, H. N., Huang, S., & Smerdon, J. E. (2006). Five centuries of climate change in Australia: The view from underground. *Journal of Quaternary Science*, 21(7), 701–706. <https://doi.org/10.1002/jqs.1060>
- Popov, Y. A., Pribnow, D., Sass, J. H., Williams, C. F., & Burkhardt, H. (1999). Characterization of rock thermal conductivity by high-resolution optical scanning. *Geothermics*, 28(2), 253–276. [https://doi.org/10.1016/s0375-6505\(99\)00007-3](https://doi.org/10.1016/s0375-6505(99)00007-3)
- Rath, V., González Rouco, J. F., & Goosse, H. (2012). Impact of postglacial warming on borehole reconstructions of last millennium temperatures. *Climate of the Past*, 8(3), 1059–1066. <https://doi.org/10.5194/cp-8-1059-2012>
- Rath, V., & Mottaghay, D. (2007). Smooth inversion for ground surface temperature histories: Estimating the optimum regularization parameter by generalized cross-validation. *Geophysical Journal of the Royal Astronomical Society*, 171(3), 1440–1448. <https://doi.org/10.1111/j.1365-246x.2007.03587.x>
- Sekiguchi, K. (1984). A method for determining terrestrial heat flow in oil basinal areas. *Tectonophysics*, 103(1–4), 67–79. [https://doi.org/10.1016/0040-1951\(84\)90075-1](https://doi.org/10.1016/0040-1951(84)90075-1)

- Shi, Y., Jiang, G., Zhang, X., Yuan, Z., Wang, Z., Qiu, Q., & Hu, S. (2018). Present temperature field characterization and geothermal resource assessment in the Harbin Area, Northeast China. *Energy Exploration & Exploitation*, 54861490.
- Vogt, C., Mottaghy, D., Rath, V., Marquart, G., Dijkshoorn, L., Wolf, A., & Clauser, C. (2014). Vertical variation in heat flow on the Kola Peninsula: Palaeoclimate or fluid flow? *Geophysical Journal International*, 199(2), 829–843. <https://doi.org/10.1093/gji/ggu282>
- Wang, C., Feng, Z., Zhang, L., Huang, Y., Cao, K., Wang, P., & Zhao, B. (2013). Cretaceous paleogeography and paleoclimate and the setting of SKI borehole sites in Songliao Basin, northeast China. *Palaeogeography, Palaeoclimatology, Palaeoecology*, 385, 17–30. <https://doi.org/10.1016/j.palaeo.2012.01.030>
- Wang, P., Mattern, F., Didenko, N. A., Zhu, D., Singer, B., & Sun, X. (2016). Tectonics and cycle system of the Cretaceous Songliao Basin: An inverted active continental margin basin. *Earth-Science Reviews*, 159, 82–102. <https://doi.org/10.1016/j.earscirev.2016.05.004>
- Wu, Q. F., & Xie, Y. Z. (1985). Geothermal heat flow in the Songhuajiang-Liaoning basin. *Seismology and Geology*, 7(02), 59–64. (in Chinese).
- Zhu, H. L. (2011). Research on the sedimentary geothermal resources in North Songliao Basin. Ph.D. thesis, Northeast Petroleum University. (in Chinese).
- Zou, C., Zhang, X., Zhao, J., Peng, C., Zhang, S., Li, N., et al. (2018). Scientific results of geophysical logging in the upper Cretaceous Strata, CCSD SK-2 east borehole in the Songliao Basin of northeast China. *Acta Geoscientia Sinica*, 39(06), 679–690. (in Chinese).

References From the Supporting Information

- Carslaw, H. S., & Jaeger, J. C. (1959). *Conduction of heat in solids* (p. 99). Oxford University Press.
- Su, Y. (2021). Genesis and rational development of typical geothermal field in the Songliao Basin: A case study of Lindian geothermal field. Ph.D. thesis, Jinlin University. (in Chinese).